

# MorphAny3D: Unleashing the Power of Structured Latent in 3D Morphing

Xiaokun Sun<sup>1</sup>, Zeyu Cai<sup>1</sup>, Hao Tang<sup>2</sup>, Ying Tai<sup>1</sup>, Jian Yang<sup>1</sup>, Zhenyu Zhang<sup>1\*</sup>

<sup>1</sup>Nanjing University <sup>2</sup>Peking University

\*Corresponding Author

xiaokun\_sun@smail.nju.edu.cn, caizeyu010612@gmail.com, bjdxtanghao@gmail.com

{yingtai, csjyang}@nju.edu.cn, zhangjesse@foxmail.com



Figure 1. **MorphAny3D** enables smooth, semantically coherent, and aesthetically pleasing transitions from source objects (first column) to target objects (last column), even when they share no semantic or visual relationship (e.g., bee to biplane in the second row).

## Abstract

3D morphing remains challenging due to the difficulty of generating semantically consistent and temporally smooth deformations, especially across categories. We present *MorphAny3D*, a training-free framework that leverages Structured Latent (SLAT) representations for high-quality 3D morphing. Our key insight is that intelligently blending source and target SLAT features within the attention mechanisms of 3D generators naturally produces plausible morphing sequences. To this end, we introduce *Morphing Cross-Attention (MCA)*, which fuses source and target information for structural coherence, and *Temporal-Fused Self-Attention (TFSA)*, which enhances temporal consistency by incorporating features from preceding frames. An orientation correction strategy further mitigates the pose ambiguity within the morphing steps. Extensive experiments show that our method generates state-of-the-art morphing sequences, even for challenging cross-category cases. *MorphAny3D* further supports advanced applications such

as decoupled morphing and 3D style transfer, and can be generalized to other SLAT-based generative models. Project page: <https://xiaokunsun.github.io/MorphAny3D.github.io/>.

## 1. Introduction

Morphing [43, 77, 78] refers to the visual effect of seamlessly transforming a source into a target through a smooth, plausible, and aesthetic deformation sequence. This foundational technique is widely used in animation, film, and game design to enhance creative expression. Based on input dimensionality, morphing is categorized into 2D morphing [2, 4, 36, 91] and 3D morphing [17, 20, 38, 70, 84]. While 2D morphing has advanced significantly with diffusion models [30, 59, 64, 65], 3D morphing remains challenging due to the inherent complexity of modeling smooth and reasonable deformations in three dimensions.

Most existing 3D morphing approaches follow a two-stage paradigm: (1) establishing dense correspon-

dences [67, 72] between source and target objects using hand-crafted sparse landmarks [17, 60], functional maps [57], optimal transport [63], data priors [20], or extracted 2D features [50]; and (2) interpolating between these correspondences to generate intermediate shapes. While effective in constrained settings, such matching-based methods face several critical limitations. First, they typically prioritize geometric deformation while ignoring the concurrent evolution of textures. Second, they often exhibit limited generalization, particularly in cross-category transformations (e.g., morphing a chair into a car). As shown in Fig. 2-(a), inaccurate correspondence estimation frequently leads to structurally implausible morphing results.

Recent advances in feed-forward 3D generation frameworks [47, 68, 80, 82, 89, 92, 94] have substantially improved the quality and fidelity of 3D synthesis. Notably, Trellis [82] achieves diverse and high-fidelity 3D generation through its Structured Latent (SLAT) representation. Owing to SLAT’s explicit and regular structure, it shows strong potential for training-free applications such as 3D editing [37, 88], stylization [55], and scene modeling [13]. A naive strategy for 3D morphing with SLAT involves first generating a 2D morphing sequence and then lifting each frame independently into 3D using Trellis. However, as illustrated in Fig. 2-(b), this approach fails to ensure temporal consistency due to frame-wise generation and often misrepresents complex 3D deformations. A strategy that is more deeply integrated with the generative framework is to directly interpolate the initial noise and conditional features of Trellis, similar to generative-prior-based morphing methods [84, 91]. Yet, as shown in Fig. 2-(c), this strategy lacks explicit constraints on structural plausibility and temporal continuity, often producing suboptimal morphing quality. In summary, while the SLAT representation offers compelling opportunities for 3D morphing, achieving smooth, high-fidelity, and temporally coherent 3D morphing within modern SLAT-based generative frameworks remains an open and pressing challenge.

To address these challenges, we present **MorphAny3D**, a novel and robust training-free 3D morphing framework built upon the SLAT representation. As demonstrated in Fig. 1 and Fig. 2-(d), MorphAny3D fully utilizes the 3D generative prior embedded in SLAT to produce structurally plausible and temporally smooth morphing sequences between diverse object categories. Our methodology stems from a key observation: rather than interpolating at the noise or condition level, directly aggregating SLAT features within attention mechanisms yields more reasonable and visually smooth 3D deformations. Guided by this insight, we introduce two core attention-based components: (1) Morphing Cross-Attention (MCA): intelligently fuses information from the source and target objects in the cross-attention layers, ensuring the structural coherence and

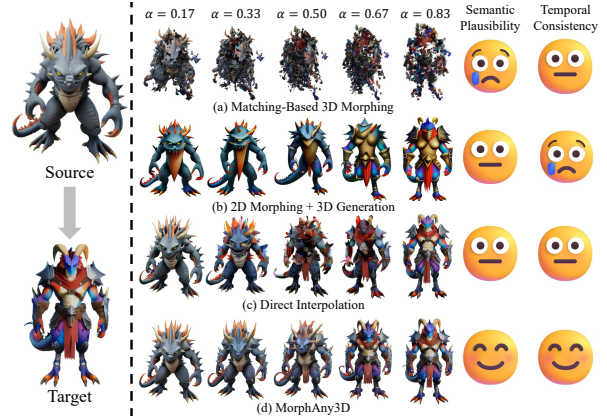


Figure 2. Comparison of different 3D morphing strategies. (a) Matching-Based 3D Morphing; (b) 2D Morphing + 3D Generation; (c) Direct Interpolation; (d) MorphAny3D. Our method leverages the powerful SLAT to achieve semantically plausible and temporally smooth 3D morphing without any training.  $\alpha \in [0, 1]$  is the deformation weight controlling the morphing progress.

aesthetics of the deformation. (2) Temporal-Fused Self-Attention (TFSA): enhances temporal coherence by incorporating SLAT features from the previous morphing frame into the self-attention mechanism, enabling smooth transitions over time. Furthermore, we propose an orientation correction strategy inspired by the orientation distribution patterns of SLAT-based 3D objects, which effectively resolves abrupt orientation shifts during the morphing process. Extensive experiments demonstrate that our method generates more plausible, smoother, and aesthetically superior 3D morphing sequences compared to existing approaches. Beyond basic morphing, MorphAny3D natively supports advanced applications such as decoupled morphing and 3D stylization, and it can be seamlessly transferred to other SLAT-based models.

Our main contributions are summarized as follows:

- We propose MorphAny3D, the first training-free 3D morphing framework based on Structured Latent (SLAT), capable of generating smooth and semantically coherent deformations across diverse 3D object categories.
- Inspired by SLAT fusion patterns in attention mechanisms, we propose Morphing Cross-Attention and Temporal-Fused Self-Attention—two key components that leverage SLAT features across objects and frames to improve morphing quality and temporal consistency.
- Drawing on the statistical orientation distributions of SLAT-based 3D objects, we propose an orientation correction strategy to mitigate abrupt orientation changes, further enhancing morphing smoothness.

## 2. Related Work

**2D Morphing.** Image morphing [36, 42, 43, 62, 96] has long been studied in computer vision and graphics due to its broad applications. Traditional methods [36, 42, 62, 96]

rely on hand-crafted features to establish image correspondences, followed by gradual blending to produce smooth transitions. However, they often fail to generate plausible, novel content and are prone to artifacts such as ghosting. With the advent of deep learning, data-driven approaches [2, 23] have improved results by learning 2D generative priors. Nevertheless, their limited model capacity makes cross-category morphing challenging. The recent success of diffusion models [30, 64, 65] has enabled high-fidelity and diverse image generation. By leveraging pre-trained text-to-image models [59], several works [4, 27, 74, 86, 91] have significantly enhanced morphing quality across different categories. Despite these advances, extending such smooth and semantically coherent transformations to 3D content remains an open challenge.

**3D Morphing.** Most 3D morphing methods rely on correspondences between source and target shapes, followed by the interpolation of matched 3D primitives. The core difficulty lies in accurate 3D matching [12, 61, 67, 72]. Early methods approach this from an axiomatic perspective, incorporating theories such as optimal transport [19, 63, 70] and functional maps [18, 53, 57, 58] to compute correspondences within the same category. In the deep learning era, one line of work [3, 20, 95] adopts a data-driven paradigm, enabling the prediction of 3D correspondences using curated 3D datasets. Another category [16, 25, 38, 44, 66] leverages powerful 2D feature extractors [52, 56, 59] to establish 3D correspondences in a zero-shot manner. However, these methods struggle to reliably find correspondences across diverse object categories, limiting the practicality of matching-based 3D morphing.

3DMorpher [84] improves cross-category morphing performance by incorporating 3DGS-based 3D generative priors. However, it cannot handle complex geometries due to limitations in its base generator. Moreover, 3DGS-based outputs are not compatible with most commercial 3D software [1, 22, 24]. In this work, inspired by Trellis [82]—a milestone in 3D generation—we propose a series of simple yet effective modules based on its SLAT representation to achieve aesthetically pleasing and semantically coherent 3D morphing without any training.

**3D Generative Models.** Advances in 2D diffusion models [30, 45, 48, 54, 64, 65] and the availability of large-scale 3D datasets [10, 11] have driven rapid progress in 3D generation [7–9, 28, 31, 32, 34, 35, 39–41, 46, 47, 68, 69, 75, 79–83, 85, 87, 89, 90, 92–94]. Among these, Trellis [82] stands out as a groundbreaking method for native 3D generation. Its proposed Structured LATent (SLAT) representation not only efficiently encodes rich visual features but is also easily modeled and understood within modern generative frameworks. Crucially, SLAT possesses a regular and explicit structure, offering superior extensibility compared to implicit or irregular representations such as VecSet [89],

NeRF [49], or 3DGS [33]. A growing body of follow-up work demonstrates that SLAT can be directly transferred—without retraining—to various downstream tasks, including 3D editing [37, 88], stylization [55], correspondence estimation [15], articulated object modeling [5], scene generation [13], and world synthesis [6, 21]. Despite its strong generalization ability, SLAT has not yet been explored for 3D morphing. In this paper, we bridge this gap by analyzing fusion rules of SLAT features in cross-/self-attention blocks, and propose lightweight yet solid modules and strategies that fully unlock the potential of SLAT for high-quality, training-free 3D morphing.

## 3. Methodology

### 3.1. Preliminaries

**Trellis** [82] is a robust feed-forward 3D generative model that produces diverse, high-fidelity 3D assets from text or image prompts. Its core encodes 3D models into the Structured LATent (SLAT) representation, i.e., a set of local latent vectors  $\{(z_i, p_i)\}_{i=1}^L$  anchored at active sparse voxels  $p_i$  on the object surface, where each  $z_i \in \mathbb{R}^C$  captures fine-scale geometry and appearance. Trellis employs a two-stage generation pipeline based on rectified flow models [45] tailored for SLAT generation: (1) Sparse Structure (SS) Stage: SS flow transformer estimates a  $64^3$  voxel grid to identify the sparse structure  $P = \{p_i\}_{i=1}^L$  representing the global shape of assets. (2) Structured Latent (SLAT) Stage: SLAT flow transformer predicts the local latent vectors  $Z = \{z_i\}_{i=1}^L$  for the voxels identified in the SS stage, producing rich geometry and texture details. Finally, the generated SLAT is decoded into standard 3D representations such as meshes, NeRF [49], or 3DGS [33]. In this work, we adopt the image-to-3D variant of Trellis [82], as image conditions facilitate modeling finer details. Notably, as shown in Sec. 4.5, our method generalizes seamlessly to other SLAT-based models with different input modalities.

**Attention** [73] mechanism is a fundamental component in modern generative models [48, 54] and is formulated as:

$$\text{Attn}(Q, K, V) = \text{Softmax}\left(\frac{QK^T}{\sqrt{d_k}}\right)V, \quad (1)$$

where  $Q$  is the query features derived from the latent feature  $f$ , while  $K$  and  $V$  are the key and value features obtained from either external conditions (cross-attention) or the latent feature itself (self-attention).

### 3.2. Overview

Given a source object  $x^{\text{src}}$  and a target object  $x^{\text{tgt}}$ , our goal is to generate a smooth, high-quality morphing sequence  $\{x^n\}_{n=0}^N$  that gradually transforms  $x^{\text{src}}$  into  $x^{\text{tgt}}$  using the SLAT representation from Trellis [82]. Both objects may be real 3D assets or Trellis-synthesized. For real assets,

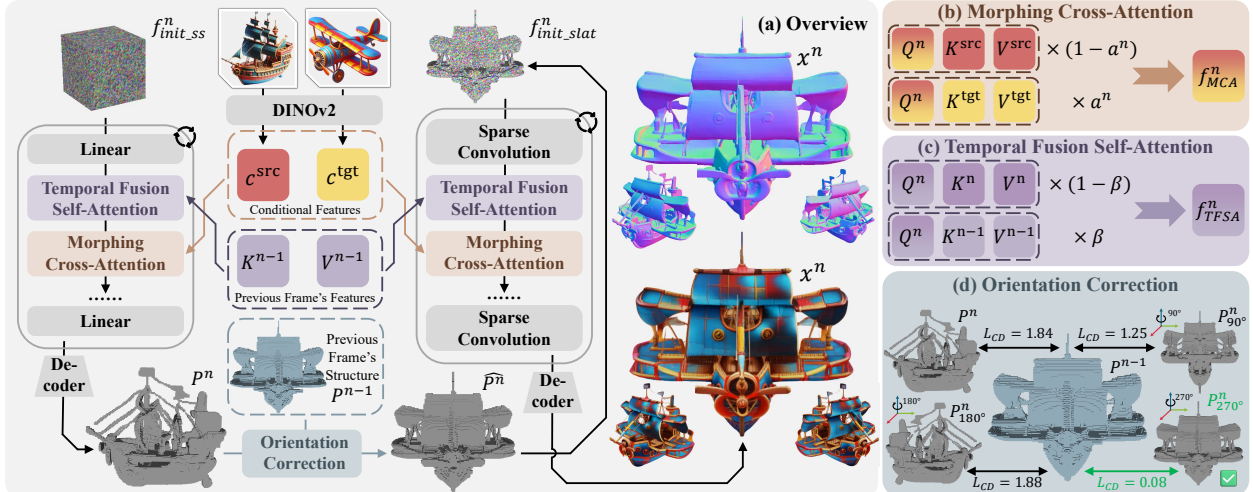


Figure 3. (a) Overview of our method. MorphAny3D generates a smooth and high-quality morphing sequence between diverse object categories by leveraging the SLAT representation without any training. (b) Morphing Cross-Attention (MCA) fuses information from the source and target objects in the cross-attention layers to ensure the structural coherence and aesthetics of the deformation. (c) Temporal-Fused Self-Attention (TFSA) enhances temporal smoothness by incorporating SLAT features from the previous morphing frame into the self-attention mechanism, enabling smooth transitions over time. (d) An orientation correction strategy inspired by statistical orientation distribution patterns in Trellis-generated assets is proposed to resolve abrupt orientation shifts.

we obtain their initial noised latents  $f_{init}^{src}$  and  $f_{init}^{tgt}$ , and image conditions  $c^{src}$ ,  $c^{tgt}$  via 3D inversion [37]. Here, the latent  $f = (f_{ss}, f_{slat})$  for each object corresponds to Trellis’s SS and SLAT stages. For Trellis-generated assets, we reuse cached initial features and conditions from the original generation. The initial noisy feature for frame  $n$ ,  $f_{init}^n$ , is computed by spherical interpolation [91] with a deformation weight  $\alpha^n \in [0, 1]$ , ensuring  $x^0 = x^{src}(\alpha^0 = 0)$  and  $x^N = x^{tgt}(\alpha^N = 1)$ . We set  $N = 49$  (50 frames) with linearly spaced  $\alpha^n = n/N$ . Further details are provided in our Supp. Mat. Fig. 3-(a) shows the MorphAny3D overview. Based on observed SLAT feature blending patterns in cross-/self-attention blocks (Sec. 3.3, Fig. 4), we introduce two key components to improve morphing plausibility and temporal coherence: Morphing Cross-Attention (Sec. 3.4, Fig. 3-(b)) and Temporal-Fused Self-Attention (Sec. 3.5, Fig. 3-(c)). We also propose an orientation correction strategy (Sec. 3.6, Fig. 3-(d)) derived from statistical analysis of orientation distributions in Trellis outputs to suppress abrupt pose shifts.

### 3.3. SLAT Fusion Patterns in Attention Mechanism

As shown in Fig. 2, naively applying SLAT to 3D morphing yields poor transitions, highlighting the need to understand how SLAT features influence the morphing process. Prior work [84, 91] shows that fusing source and target keys and values in attention greatly improves 2D/3D morphing quality and continuity:

$$\text{KV-Fused-Attn}(Q^n, K^{src/tgt}, V^{src/tgt}) = \text{Attn}(Q^n, (1 - \alpha^n)K^{src} + \alpha^n K^{tgt}, (1 - \alpha^n)V^{src} + \alpha^n V^{tgt}), \quad (2)$$

where  $Q^n$  comes from frame- $n$  latent features  $f^n$ , and  $K^{src/tgt}$  and  $V^{src/tgt}$  are derived from image conditions (cross-attention) or latent features (self-attention) of source and target objects, respectively. This fusion is shared across all diffusion timesteps and generation stages; we omit corresponding indices for brevity. Given the poor performance of naive SLAT interpolation and the success of KV fusion, we extend this strategy to Trellis’s cross-attention (CA) and self-attention (SA), yielding KV-Fused CA and KV-Fused SA. We quantitatively evaluate methods on a test set using FID (lower = more plausible) and PPL (lower = smoother) (Fig. 4-(a); see Sec. 4.1 for evaluation details) and qualitatively compare fusion strategies in Fig. 4-(b, c, d).

From these results, we draw three key observations: (1) KV-Fused CA significantly enhances the structural and semantic plausibility of 3D morphing by fusing 2D conditions from the source and target objects within cross-attention (the lowest FID). However, it fails to eliminate localized implausible artifacts, as shown in the orange box of Fig. 4-(b). (2) KV-Fused SA effectively improves the smoothness and continuity of the morphing sequence by aggregating 3D latent features from the source and target objects within self-attention (the lowest PPL). (3) Yet, simultaneously applying KV-fused CA and KV-fused SA—while aiming to maximize both plausibility and smoothness—compromises the plausibility of the resulting deformation (see Fig. 4-(d)). These results indicate that while SLAT feature blending benefits morphing, naive combination harms the plausibility-smoothness trade-off. To address this, we propose two tailored modules—Morphing Cross-Attention and Temporal-Fused Self-Attention—that preserve the advantages of fusion while avoiding its pitfalls.

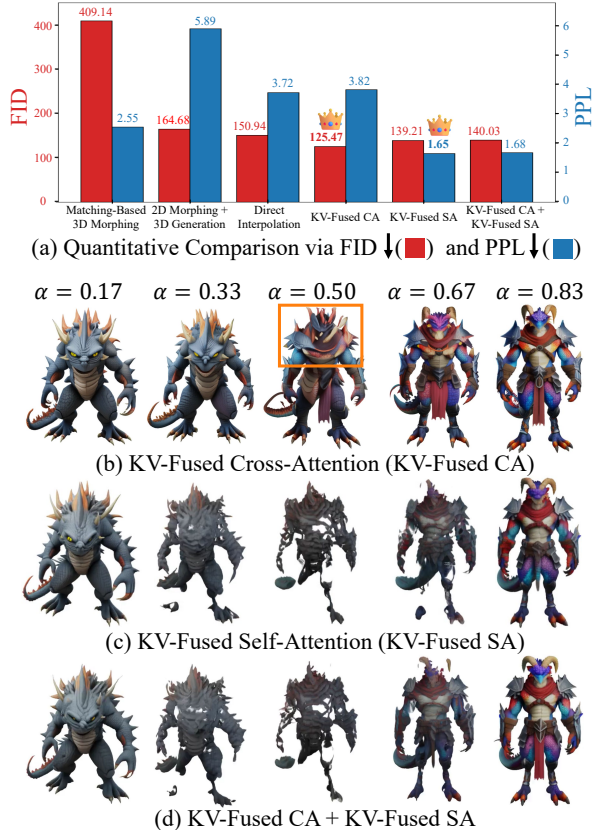


Figure 4. Analysis of SLAT fusion patterns in attention for 3D morphing. (a) FID (plausibility) and PPL (smoothness) comparison. (b, c, d) Qualitative results of different fusion strategies (same case as Fig. 2).

### 3.4. Morphing Cross-Attention (MCA)

We hypothesize that the local irrational structure in KV-Fused CA is caused by patch-wise blending of source and target 2D conditions, which introduces ambiguous semantics that mislead the generation model. Specifically, the blended keys and values in cross-attention are derived from patch-wise DINOv2 [52] features. However, spatially aligned patches between source and target images often lack semantic correspondence, leading to distorted outputs. To verify this hypothesis, we visualize the cross-attention maps of head SLAT features (marked by red stars) in Fig. 5. The attention maps from vanilla CA (second and third columns) correctly focus on the head regions in the input conditions (indicated by pink stars). In contrast, KV-Fused CA (fourth column) erroneously attends to background regions (highlighted by an orange box), subsequently using semantically mismatched features to guide head SLAT generation—resulting in local structural distortions. To address this issue, we propose Morphing Cross-Attention (MCA) (Fig. 3-(b)). Instead of blending keys and values prior to the attention computation, MCA computes separate attention outputs for the source and target objects and then com-

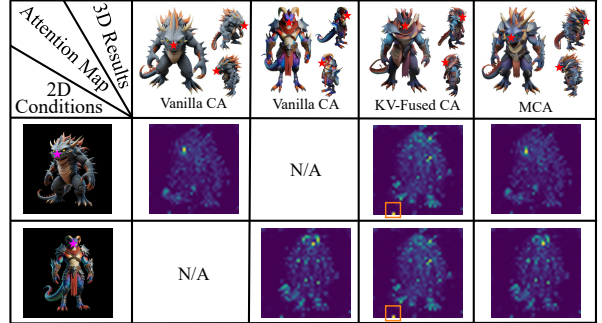


Figure 5. Attention maps visualization for different attention mechanisms. Red stars denote head SLAT features; pink stars mark their corresponding input regions. Orange boxes highlight KV-Fused CA’s incorrect attention focus. MCA preserves correct, semantically consistent attention and avoids KV-Fused CA’s artifacts shown in Fig. 4-(b).

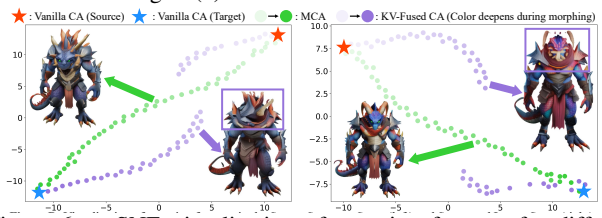


Figure 6. t-SNE visualization of attention features for different attention mechanisms in the SS Stage (left) and SLAT Stage (right). Obviously, MCA exhibits a stable, smooth feature trajectory, whereas KV-Fused CA’s is erratic and interrupted.

bins them to produce the final feature  $f_{MCA}^n$ :

$$MCA(Q^n, K^{\text{src}/\text{tgt}}, V^{\text{src}/\text{tgt}}) = (1 - \alpha^n) \text{Attn}(Q^n, K^{\text{src}}, V^{\text{src}}) + \alpha^n \text{Attn}(Q^n, K^{\text{tgt}}, V^{\text{tgt}}). \quad (3)$$

As shown in the last column of Fig. 5, MCA preserves accurate attention on semantically consistent regions by processing source and target features independently, thereby avoiding the artifacts observed in KV-Fused CA. This improvement is further corroborated in Sec. 4.3.

Furthermore, we verified MCA’s efficacy via feature distribution analysis. Fig. 6 shows t-SNE [71] visualizations of average output features from vanilla CA, MCA, and KV-Fused CA across all blocks and diffusion timesteps in the SS and SLAT stages (green/purple deepen during morphing). Notably, MCA exhibits a stable, smooth trajectory, whereas KV-Fused CA yields an erratic, interrupted path. Combined with Fig. 5, this reveals that naive KV fusion disrupts conditions’ semantic consistency, causing unstable 3D morphing (interrupted purple trajectory) and chaotic outputs (purple arrow). In contrast, MCA preserves accurate, semantically consistent attention maps, enabling smooth, plausible 3D deformations (stable green trajectory and arrow).

### 3.5. Temporal-Fused Self-Attention (TFSA)

Although MCA yields structurally coherent and visually plausible deformations, temporal smoothness re-

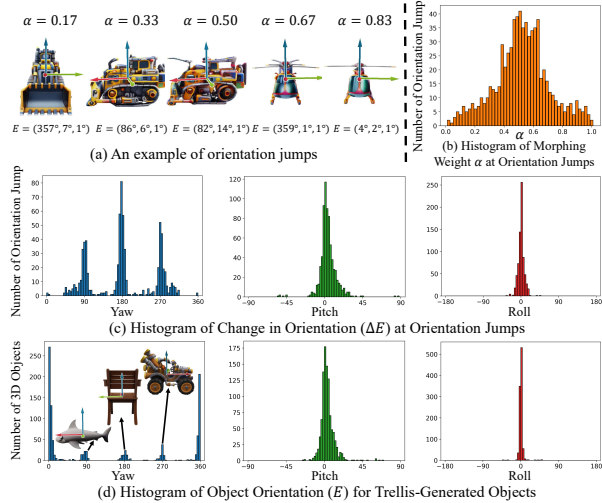


Figure 7. (a) Example of abrupt orientation change during morphing. (b) Distribution of  $\alpha$  at orientation jumps, peaking near intermediate stages. (c) Adjacent-frame orientation changes  $\Delta E$  at orientation jumps, dominated by  $90^\circ$ ,  $180^\circ$ , and  $270^\circ$  yaw shifts. (d) Orientation distribution of Trellis-generated objects, showing non-canonical poses clustered at the same yaw angles.

mains limited due to the frame-wise independence inherent in standard 3D generators. To address this limitation—and building on insights from KV-Fused SA discussed in Sec. 3.3—we propose Temporal-Fused Self-Attention (TFSA). As illustrated in Fig. 3-(c), TFSA promotes temporally consistent 3D morphing by incorporating features from previously generated frames into the self-attention mechanism. Specifically, when generating the  $n$  frame, TFSA fuses attention outputs from current and previous frames’ keys and values to produce the output  $f_{TFSA}^n$ :

$$TFSA(Q^n, K^n, V^n, K^{n-1}, V^{n-1}) = (1 - \beta) \text{Attn}(Q^n, K^n, V^n) + \beta \text{Attn}(Q^n, K^{n-1}, V^{n-1}), \quad (4)$$

where  $\beta \in [0, 1]$  controls the influence of the prior frame. We empirically set  $\beta = 0.2$ . Unlike the KV-Fused SA in Fig. 4-(e, f)—which blends source and target features—TFSA fuses features from already plausible neighboring morphing frames, preserving semantic fidelity while enhancing smoothness, as shown in Sec. 4.3 and Fig. 9-(b).

### 3.6. Orientation Correction

Morphing often suffers from abrupt orientation changes (i.e., orientation jumps)—especially in intermediate stages—causing visually jarring transitions (Fig. 7-(a)). We represent orientation via the Z-Y-X Euler angles  $E = (\text{yaw}, \text{pitch}, \text{roll})$  (in degrees), estimated using OrientAnything [76]. An orientation jump is flagged when the adjacent-frame angular difference  $\Delta E$  exceeds  $45^\circ$ , a threshold accounting for estimation noise.

Analyzing 200 sequences (50 frames each) generated with MCA and TFSA, we find that jumps concentrate

around  $\alpha \approx 0.5$  (Fig. 7-(b)), where the conditional features are the most ambiguous. Moreover,  $\Delta E$  is strongly biased toward yaw rotations of  $90^\circ$ ,  $180^\circ$ , and  $270^\circ$ , with negligible pitch/roll changes (Fig. 7-(c)), suggesting a systematic bias rather than randomness. We hypothesize that this stems from Trellis’s internal pose prior. To verify, we estimate the orientations of 1,000 Trellis-generated objects (Fig. 7-(d)): while most adopt canonical poses, non-canonical ones cluster precisely at the same yaw angles (see cases in Fig. 7-(d)-Yaw)—confirming the link between orientation jumps and Trellis’s learned pose distribution.

Based on these observations, we propose a lightweight orientation correction strategy to mitigate abrupt orientation changes (Fig. 3-(d)). After generating the sparse structure  $P^n$  in the SS stage, we create four yaw-rotated candidates:  $P^n$ ,  $P_{90^\circ}^n$ ,  $P_{180^\circ}^n$ , and  $P_{270^\circ}^n$ . We select the candidate that minimizes the Chamfer Distance (CD) to the previous frame’s structure  $P^{n-1}$  as the corrected structure  $\hat{P}^n$ , which is then passed to the SLAT flow transformer. Since jumps occur mainly mid-sequence (Fig. 7-(b)), this leverages early stable poses to correct later errors. When no jump occurs, the unrotated  $P^n$  yields the lowest CD and is retained—ensuring non-intrusiveness. As shown in Sec. 4.3, this significantly improves temporal smoothness without sacrificing fidelity.

## 4. Experiments

Due to space limits, we report key settings and results; **full details are in the Supp. Mat.** We render RGB views from 3DGS and normal maps from Mesh representations.

### 4.1. Experimental Settings

**Implementation Details.** Our method uses Image-to-3D Trellis [82] without retraining or hyperparameter tuning. Experiments were conducted on a single A6000 GPU. Generating each frame takes 30s with 24GB of memory.

**Baselines.** We compare four types: (1) Matching-based 3D morphing of 3D or SLAT features (*3DInterp*, *SLAT-Interp*, and use DenseMatcher [95] for correspondence); (2) 2D morphing (DiffMorpher [91], FreeMorph [4]) is lifted to 3D via Trellis; (3) Direct interpolation of noise and conditions (*DirectInterp*); (4) Modern 3D morphing method—MorphFlow [70]. Since 3DMorpher [84] has not released its full code, we provide only a qualitative comparison in our Supp. Mat.

**Evaluation Metrics.** We evaluate 50 diverse source-target pairs from real 3D datasets [14, 37] and Trellis-generated assets using four metrics: (a) FID [29] measures visual plausibility by comparing rendered frames to originals; (b) Perceptual Path Length (PPL) and Perceptual Distance Variance (PDV) [91] assess transition smoothness and temporal homogeneity via average perceptual change and its variance between adjacent frames; (c) Aesthetics Scores (AS) uses

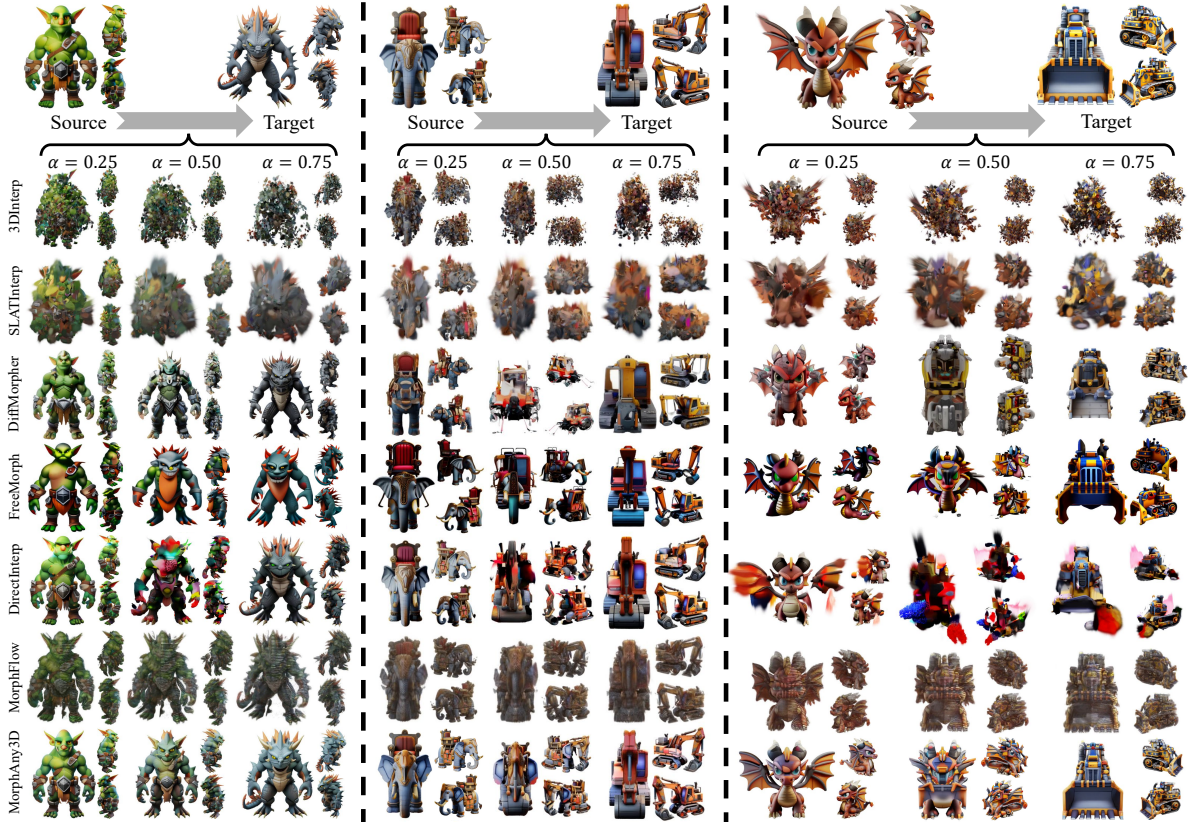


Figure 8. Qualitative comparisons. MorphAny3D generates smooth, high-quality 3D morphing sequences across diverse object categories. **More results are provided in our Supp. Mat.**

vision-language models [26, 51] to rank visual appeal; (d) User Preference (UP) is gathered through a user study evaluating quality, smoothness, and realism.

## 4.2. Evaluation

**Qualitative Results.** As shown in Fig. 8, MorphAny3D generates smooth, high-quality 3D morphing sequences across diverse categories, outperforming all baselines. Matching-based methods (e.g., 3DInterp, SLATInterp, MorphFlow) yield smooth, but often implausible or semantically incoherent transitions. 2D-first approaches (DiffMorpher, FreeMorph) leverage strong 2D priors for structural plausibility but suffer from poor 3D temporal consistency, leading to jerky sequences. DirectInterp’s feature fusion is ill-suited to SLAT, resulting in suboptimal deformations. In contrast, our method unleashes the potential of 3D generative priors in SLAT to produce temporally smooth, semantically meaningful, and visually faithful morphs. For example, in the elephant-to-excavator case (Fig. 8), it implicitly aligns the trunk with the boom, creating a coherent hybrid that seamlessly blends both concepts.

**Quantitative Results.** As shown in Tab. 1, MorphAny3D achieves state-of-the-art performance, obtaining the best scores in FID, PDV, AS, and UP, and the second-best PPL. Matching-based methods achieve smoothness via linear in-

Table 1. Quantitative comparison. Best and second-best in **bold** and underlined.

Method	FID ↓	PPL ↓	PDV ↓	AS (%) ↑	UP (%) ↑
3DInterp [95]	409.14	2.55	<b>0.0006</b>	1.00	0.61
SLATInterp [95]	348.31	6.53	0.0010	0.00	1.43
DiffMorpher [91]	208.08	6.65	0.0021	5.00	0.82
FreeMorph [4]	164.68	5.89	0.0027	<u>11.00</u>	3.27
DirectInterp	150.94	3.72	0.0039	2.00	<u>5.51</u>
MorphFlow [70]	284.96	<b>2.41</b>	<b>0.0009</b>	0.00	1.63
MorphAny3D	<b>111.95</b>	<u>2.47</u>	<b>0.0006</b>	<b>81.00</b>	<b>86.73</b>

Table 2. Ablation study on key components of MorphAny3D.

Method	FID ↓	PPL ↓	PDV ↓
KV-Fused CA	125.47	3.82	0.0013
MCA	112.18	3.66	0.0010
MCA + TFSA	<u>113.22</u>	2.87	<b>0.0007</b>
MCA + TFSA + OC	<b>111.95</b>	<b>2.47</b>	<b>0.0006</b>

terpolation but suffer from poor plausibility, as evidenced by an extremely high FID. Our method significantly improves plausibility and visual quality with only a marginal smoothness trade-off—its PPL is just 0.06 above the lowest.

## 4.3. Ablation Study

**Effectiveness of MCA.** Fig. 9-(a) shows that MCA suppresses local artifacts (blue box) in KV-Fused CA and improves plausibility. FID drops from 125.47 to 112.18 (Tab. 2). **Effectiveness of TFSA.** Fig. 9-(b) shows improved temporal coherence—e.g., stable crab claws and eyes (green/red boxes). PPL and PDV decrease to 2.87 and

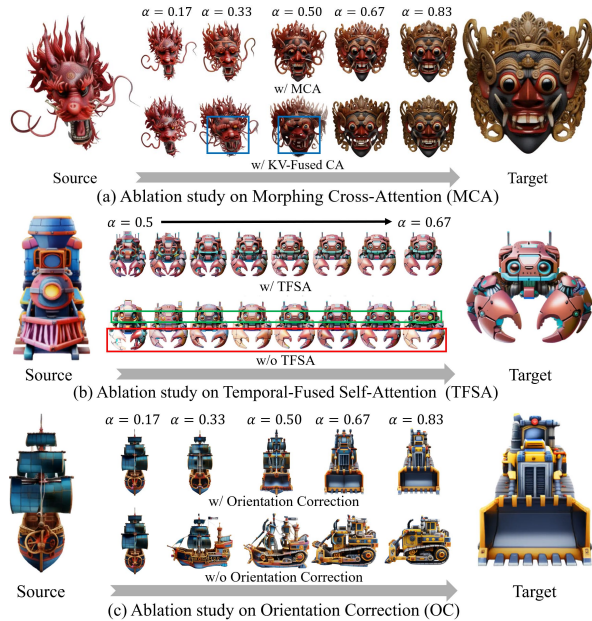


Figure 9. Ablation study on (a) MCA, (b) TFSA, and (c) OC.

0.0007. **Effectiveness of Orientation Correction (OC).** Fig. 9-(c) shows that OC mitigates orientation jumps. Quantitatively, it further reduces PPL to 2.47 and PDV to 0.0006.

#### 4.4. Applications

**Disentangled 3D Morphing.** By applying our method selectively to Trellis’s SS and SLAT stages, we decouple the global structure from local details. Fig. 10-(a) shows sequences that preserve the source structure with target details (or vice versa). **Dual-Target 3D Morphing.** Assigning different targets to SS and SLAT enables morphing toward two concepts simultaneously. Fig. 10-(b) shows one target shaping structure, the other detail. **3D Style Transfer.** Using a style image as the SLAT target transfers style while preserving source structure and aesthetics (Fig. 10-(c)).

#### 4.5. Generalization Ability

We apply MorphAny3D to other SLAT-based models—Hi3DGen [87] and Text-to-3D Trellis [82]. As shown in Fig. 11, it consistently produces smooth, high-quality morphs, confirming its versatility.

### 5. Conclusion

We present MorphAny3D, a training-free 3D morphing framework based on Trellis’s SLAT representation. By analyzing SLAT fusion in attention, we introduce Morphing Cross-Attention (MCA)—fusing source and target features for structural and semantic fidelity—and Temporal-Fused Self-Attention (TFSA)—leveraging prior frames for temporal coherence. We also propose an orientation correction strategy, guided by statistical pose patterns in Trellis outputs, to reduce abrupt orientation shifts. Experiments show



Figure 10. Applications: (a) Disentangled 3D morphing, (b) Dual-Target 3D Morphing and (c) 3D Style Transfer.

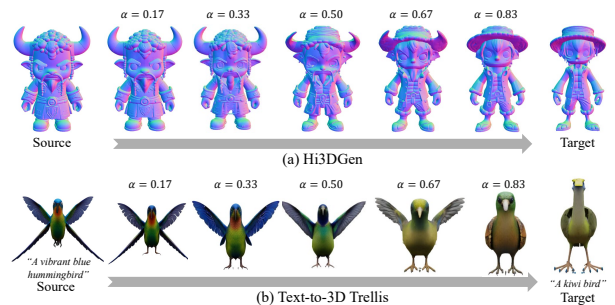


Figure 11. Generalization experiments on (a) Hi3DGen and (b) Text-to-3D Trellis.

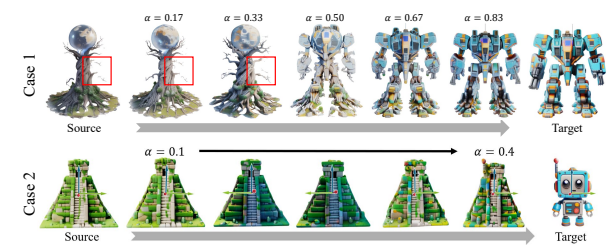


Figure 12. Failure cases.

that our method achieves state-of-the-art results in generating smooth, high-quality 3D morphing sequences across diverse object categories. It further supports advanced applications such as decoupled morphing and 3D style transfer, and readily generalizes to other SLAT-based models.

**Limitations and Future Work.** MorphAny3D inherits Trellis’s limitations and may exhibit artifacts on extremely fine structures (see red boxes of case 1 in Fig. 12). Future work could adopt stronger 3D generative backbones [28] or enhance SLAT representations to capture finer geometric details. Additionally, our orientation correction strategy may miss yaw-symmetric objects’ rotations (see case 2 in Fig. 12). Finally, the high runtime restricts its application; we plan to investigate acceleration methods like KV cache.

**Acknowledgement.** This work was supported by the NSFC under Grant No. 62376121, Basic Research Program of Jiangsu under Grant No. BK20251999, Gusu Innovation Leading Talent Program under Grant No. ZXL2025319, and Jiangsu Provincial Science & Technology Major Project under Grant No. BG2024042.

## References

- [1] Inc. Autodesk. Autodesk maya - 3d animation and modeling software. <https://www.autodesk.com/products/maya>, 2024. 3, 14
- [2] Hadar Averbuch-Elor, Daniel Cohen-Or, and Johannes Kopf. Smooth image sequences for data-driven morphing. In *Comput. Graph. Forum*, 2016. 1, 3
- [3] Dongliang Cao and Florian Bernard. Self-supervised learning for multimodal non-rigid 3d shape matching. In *Proc. IEEE Conf. Comput. Vis. Pattern Recogn.*, 2023. 3
- [4] Yukang Cao, Chenyang Si, Jinghao Wang, and Ziwei Liu. Freemorph: Tuning-free generalized image morphing with diffusion model. In *Proc. IEEE Int. Conf. Comput. Vis.*, 2025. 1, 3, 6, 7, 13
- [5] Chuhao Chen, Isabella Liu, Xinyue Wei, Hao Su, and Minghua Liu. Freeart3d: Training-free articulated object generation using 3d diffusion. *arXiv preprint arXiv:2510.25765*, 2025. 3
- [6] Hanke Chen, Yuan Liu, and Minchen Li. Trellisworld: Training-free world generation from object generators. *arXiv preprint arXiv:2510.23880*, 2025. 3
- [7] Rui Chen, Jianfeng Zhang, Yixun Liang, Guan Luo, Weiyu Li, Jiarui Liu, Xiu Li, Xiaoxiao Long, Jiashi Feng, and Ping Tan. Dora: Sampling and benchmarking for 3d shape variational auto-encoders. In *Proc. IEEE Conf. Comput. Vis. Pattern Recogn.*, 2025. 3
- [8] Yiwen Chen, Zhihao Li, Yikai Wang, Hu Zhang, Qin Li, Chi Zhang, and Guosheng Lin. Ultra3d: Efficient and high-fidelity 3d generation with part attention. *arXiv preprint arXiv:2507.17745*, 2025.
- [9] Zhaoxi Chen, Jiayang Tang, Yuhao Dong, Ziang Cao, Fangzhou Hong, Yushi Lan, Tengfei Wang, Haozhe Xie, Tong Wu, Shunsuke Saito, et al. 3dtopia-xl: Scaling high-quality 3d asset generation via primitive diffusion. In *Proc. IEEE Conf. Comput. Vis. Pattern Recogn.*, 2025. 3
- [10] Matt Deitke, Ruoshi Liu, Matthew Wallingford, Huong Ngo, Oscar Michel, Aditya Kusupati, Alan Fan, Christian Laforte, Vikram Voleti, Samir Yitzhak Gadre, et al. Objaverse-xl: A universe of 10m+ 3d objects. In *Adv. Neural Inf. Process. Syst.*, 2023. 3
- [11] Matt Deitke, Dustin Schwenk, Jordi Salvador, Luca Weihs, Oscar Michel, Eli VanderBilt, Ludwig Schmidt, Kiana Ehsani, Aniruddha Kembhavi, and Ali Farhadi. Objaverse: A universe of annotated 3d objects. In *Proc. IEEE Conf. Comput. Vis. Pattern Recogn.*, 2023. 3
- [12] Bailin Deng, Yuxin Yao, Roberto M Dyke, and Juyong Zhang. A survey of non-rigid 3d registration. In *Comput. Graph. Forum*, 2022. 3
- [13] Wenqi Dong, Bangbang Yang, Zesong Yang, Yuan Li, Tao Hu, Hujun Bao, Yuewen Ma, and Zhaopeng Cui. Hiscene: creating hierarchical 3d scenes with isometric view generation. *arXiv preprint arXiv:2504.13072*, 2025. 2, 3
- [14] Laura Downs, Anthony Francis, Nate Koenig, Brandon Kinman, Ryan Hickman, Krista Reymann, Thomas B McHugh, and Vincent Vanhoucke. Google scanned objects: A high-quality dataset of 3d scanned household items. In *International Conference on Robotics and Automation*, 2022. 6
- [15] Keyu Du, Jingyu Hu, Haipeng Li, Hao Xu, Haibing Huang, Chi-Wing Fu, and Shuaicheng Liu. Hierarchical neural semantic representation for 3d semantic correspondence. *arXiv preprint arXiv:2509.17431*, 2025. 3
- [16] Niladri Shekhar Dutt, Sanjeev Muralikrishnan, and Niloy J Mitra. Diffusion 3d features (diff3f): Decorating untextured shapes with distilled semantic features. In *Proc. IEEE Conf. Comput. Vis. Pattern Recogn.*, 2024. 3
- [17] Michal Edelstein, Danielle Ezuz, and Mirela Ben-Chen. Enigma: Evolutionary non-isometric geometry matching. *arXiv preprint arXiv:1905.10763*, 2019. 1, 2
- [18] Marvin Eisenberger, Zorah Lahner, and Daniel Cremers. Smooth shells: Multi-scale shape registration with functional maps. In *Proc. IEEE Conf. Comput. Vis. Pattern Recogn.*, 2020. 3
- [19] Marvin Eisenberger, Aysim Toker, Laura Leal-Taixé, and Daniel Cremers. Deep shells: Unsupervised shape correspondence with optimal transport. In *Adv. Neural Inf. Process. Syst.*, 2020. 3
- [20] Marvin Eisenberger, David Novotny, Gael Kerchenbaum, Patrick Labatut, Natalia Neverova, Daniel Cremers, and Andrea Vedaldi. Neuromorph: Unsupervised shape interpolation and correspondence in one go. In *Proc. IEEE Conf. Comput. Vis. Pattern Recogn.*, 2021. 1, 2, 3
- [21] Paul Engstler, Aleksandar Shtedritski, Iro Laina, Christian Rupperecht, and Andrea Vedaldi. Syncity: Training-free generation of 3d worlds. *arXiv preprint arXiv:2503.16420*, 2025. 3
- [22] Inc. Epic Games. Unreal engine - real-time 3d creation tool. <https://www.unrealengine.com/>, 2024. 3
- [23] Noa Fish, Richard Zhang, Lilach Perry, Daniel Cohen-Or, Eli Shechtman, and Connelly Barnes. Image morphing with perceptual constraints and stn alignment. In *Comput. Graph. Forum*, 2020. 3
- [24] Blender Foundation. Blender - a 3d modelling and rendering software. <https://www.blender.org/>, 2024. 3, 14
- [25] William Gao, Noam Aigerman, Thibault Groueix, Vova Kim, and Rana Hanocka. Textdeformer: Geometry manipulation using text guidance. In *ACM SIGGRAPH Asia*, 2023. 3
- [26] Google DeepMind. Gemini: A family of multimodal large language models, 2024. 7, 13
- [27] Qiyuan He, Jinghao Wang, Ziwei Liu, and Angela Yao. Aid: Attention interpolation of text-to-image diffusion. *arXiv preprint arXiv:2403.17924*, 2024. 3
- [28] Xianglong He, Zi-Xin Zou, Chia-Hao Chen, Yuan-Chen Guo, Ding Liang, Chun Yuan, Wanli Ouyang, Yan-Pei Cao, and Yangguang Li. Sparseflex: High-resolution

- and arbitrary-topology 3d shape modeling. *arXiv preprint arXiv:2503.21732*, 2025. 3, 8
- [29] Martin Heusel, Hubert Ramsauer, Thomas Unterthiner, Bernhard Nessler, and Sepp Hochreiter. Gans trained by a two time-scale update rule converge to a local nash equilibrium. In *Adv. Neural Inf. Process. Syst.*, 2017. 6, 13
- [30] Jonathan Ho, Ajay Jain, and Pieter Abbeel. Denoising diffusion probabilistic models. In *Adv. Neural Inf. Process. Syst.*, 2020. 1, 3
- [31] Yicong Hong, Kai Zhang, Jiuxiang Gu, Sai Bi, Yang Zhou, Difan Liu, Feng Liu, Kalyan Sunkavalli, Trung Bui, and Hao Tan. Lrm: Large reconstruction model for single image to 3d. *arXiv preprint arXiv:2311.04400*, 2023. 3
- [32] Team Hunyuan3D, Bowen Zhang, Chunchao Guo, Haolin Liu, Hongyu Yan, Huiwen Shi, Jingwei Huang, Junlin Yu, Kunhong Li, Penghao Wang, et al. Hunyuan3d-omni: A unified framework for controllable generation of 3d assets. *arXiv preprint arXiv:2509.21245*, 2025. 3
- [33] Bernhard Kerbl, Georgios Kopanas, Thomas Leimkühler, and George Drettakis. 3d gaussian splatting for real-time radiance field rendering. *ACM Trans. Graph.*, 2023. 3
- [34] Zeqiang Lai, Yunfei Zhao, Haolin Liu, Zibo Zhao, Qingxiang Lin, Huiwen Shi, Xianghui Yang, Mingxin Yang, Shuhui Yang, Yifei Feng, et al. Hunyuan3d 2.5: Towards high-fidelity 3d assets generation with ultimate details. *arXiv preprint arXiv:2506.16504*, 2025. 3
- [35] Yushi Lan, Shangchen Zhou, Zhaoyang Lyu, Fangzhou Hong, Shuai Yang, Bo Dai, Xingang Pan, and Chen Change Loy. Gaussiananything: Interactive point cloud latent diffusion for 3d generation. In *Proc. Int. Conf. Learn. Represent.*, 2025. 3
- [36] Seung-Yong Lee, KYUNG-YONG CHWA, James Hahn, and Sung Yong Shin. Image morphing using deformation techniques. *The Journal of Visualization and Computer Animation*, 1996. 1, 2
- [37] Lin Li, Zehuan Huang, Haoran Feng, Gengxiong Zhuang, Rui Chen, Chunchao Guo, and Lu Sheng. Voxhammer: Training-free precise and coherent 3d editing in native 3d space. *arXiv preprint arXiv:2508.19247*, 2025. 2, 3, 4, 6, 13
- [38] Mengtian Li, Yunshu Bai, Yimin Chu, Yijun Shen, Zhongmei Li, Weifeng Ge, Zhifeng Xie, and Chaofeng Chen. Gaussianmorphing: Mesh-guided 3d gaussians for semantic-aware object morphing. *arXiv preprint arXiv:2510.02034*, 2025. 1, 3
- [39] Weiyu Li, Jiarui Liu, Hongyu Yan, Rui Chen, Yixun Liang, Xuelin Chen, Ping Tan, and Xiaoxiao Long. Craftsman3d: High-fidelity mesh generation with 3d native generation and interactive geometry refiner. *arXiv preprint arXiv:2405.14979*, 2024. 3
- [40] Yangguang Li, Zi-Xin Zou, Zexiang Liu, Dehu Wang, Yuan Liang, Zhipeng Yu, Xingchao Liu, Yuan-Chen Guo, Ding Liang, Wanli Ouyang, et al. Triposg: High-fidelity 3d shape synthesis using large-scale rectified flow models. *arXiv preprint arXiv:2502.06608*, 2025.
- [41] Zhihao Li, Yufei Wang, Heliang Zheng, Yihao Luo, and Bihan Wen. Sparc3d: Sparse representation and construction for high-resolution 3d shapes modeling. *arXiv preprint arXiv:2505.14521*, 2025. 3
- [42] Jing Liao, Rodolfo S Lima, Diego Nehab, Hugues Hoppe, Pedro V Sander, and Jinhui Yu. Automating image morphing using structural similarity on a halfway domain. *ACM Trans. Graph.*, 2014. 2
- [43] Jianchu Lin, Yinxi Gu, Guangxiao Du, Guoqiang Qu, Xiaobing Chen, Yudong Zhang, Shangbing Gao, Zhen Liu, and Nallappan Gunasekaran. 2d/3d image morphing technology from traditional to modern: A survey. *Information Fusion*, 2024. 1, 2
- [44] Haolin Liu, Xiaohang Zhan, Zizheng Yan, Zhongjin Luo, Yuxin Wen, and Xiaoguang Han. Stable-score: A stable registration-based framework for 3d shape correspondence. In *Proc. IEEE Conf. Comput. Vis. Pattern Recogn.*, 2025. 3
- [45] Xingchao Liu, Chengyue Gong, and Qiang Liu. Flow straight and fast: Learning to generate and transfer data with rectified flow. *arXiv preprint arXiv:2209.03003*, 2022. 3
- [46] Yuan Liu, Cheng Lin, Zijiao Zeng, Xiaoxiao Long, Lingjie Liu, Taku Komura, and Wenping Wang. Syncdreamer: Generating multiview-consistent images from a single-view image. *arXiv preprint arXiv:2309.03453*, 2023. 3
- [47] Xiaoxiao Long, Yuan-Chen Guo, Cheng Lin, Yuan Liu, Zhiyang Dou, Lingjie Liu, Yuexin Ma, Song-Hai Zhang, Marc Habermann, Christian Theobalt, et al. Wonder3d: Single image to 3d using cross-domain diffusion. In *Proc. IEEE Conf. Comput. Vis. Pattern Recogn.*, 2024. 2, 3
- [48] Nanye Ma, Mark Goldstein, Michael S Albergo, Nicholas M Boffi, Eric Vanden-Eijnden, and Saining Xie. Sit: Exploring flow and diffusion-based generative models with scalable interpolant transformers. In *Proc. Eur. Conf. Comput. Vis.*, 2024. 3
- [49] Ben Mildenhall, Pratul P. Srinivasan, Matthew Tancik, Jonathan T. Barron, Ravi Ramamoorthi, and Ren Ng. Nerf: Representing scenes as neural radiance fields for view synthesis. In *Proc. Eur. Conf. Comput. Vis.*, 2020. 3
- [50] Luca Morreale, Noam Aigerman, Vladimir G Kim, and Niloy J Mitra. Neural semantic surface maps. In *Comput. Graph. Forum*, 2024. 2
- [51] OpenAI. ChatGPT: Optimizing language models for dialogue, 2023. 7, 13
- [52] Maxime Oquab, Timothée Darcet, Théo Moutakanni, Huy Vo, Marc Szafraniec, Vasil Khalidov, Pierre Fernandez, Daniel Haziza, Francisco Massa, Alaaeldin El-Nouby, et al. Dinov2: Learning robust visual features without supervision. *arXiv preprint arXiv:2304.07193*, 2023. 3, 5
- [53] Maks Ovsjanikov, Mirela Ben-Chen, Justin Solomon, Adrian Butscher, and Leonidas Guibas. Functional maps: a flexible representation of maps between shapes. *ACM Trans. Graph.*, 2012. 3
- [54] William Peebles and Saining Xie. Scalable diffusion models with transformers. In *Proc. IEEE Int. Conf. Comput. Vis.*, 2023. 3
- [55] Zefan Qu, Zhenwei Wang, Haoyuan Wang, Ke Xu, Gerhard Hancé, and Rynson WH Lau. Stylesculptor: Zero-shot style-controllable 3d asset generation with texture-geometry dual guidance. *arXiv preprint arXiv:2509.13301*, 2025. 2, 3
- [56] Alec Radford, Jong Wook Kim, Chris Hallacy, Aditya Ramesh, Gabriel Goh, Sandhini Agarwal, Girish Sastry,

- Amanda Askill, Pamela Mishkin, Jack Clark, et al. Learning transferable visual models from natural language supervision. In *Proc. Int. Conf. Mach. Learn.*, 2021. 3
- [57] Jing Ren, Mikhail Panine, Peter Wonka, and Maks Ovsjanikov. Structured regularization of functional map computations. In *Comput. Graph. Forum*, 2019. 2, 3
- [58] Emanuele Rodola, Samuel Rota Buló, Thomas Windheuser, Matthias Vestner, and Daniel Cremers. Dense non-rigid shape correspondence using random forests. In *Proc. IEEE Conf. Comput. Vis. Pattern Recogn.*, 2014. 3
- [59] Robin Rombach, Andreas Blattmann, Dominik Lorenz, Patrick Esser, and Björn Ommer. High-resolution image synthesis with latent diffusion models. In *Proc. IEEE Conf. Comput. Vis. Pattern Recogn.*, 2022. 1, 3
- [60] Yusuf Sahilliođlu. A genetic isometric shape correspondence algorithm with adaptive sampling. *ACM Trans. Graph.*, 2018. 2
- [61] Yusuf Sahilliođlu. Recent advances in shape correspondence. *The Visual Computer*, 2020. 3
- [62] Eli Shechtman, Alex Rav-Acha, Michal Irani, and Steve Seitz. Regenerative morphing. In *Proc. IEEE Conf. Comput. Vis. Pattern Recogn.*, 2010. 2
- [63] Justin Solomon, Fernando De Goes, Gabriel Peyré, Marco Cuturi, Adrian Butscher, Andy Nguyen, Tao Du, and Leonidas Guibas. Convolutional wasserstein distances: Efficient optimal transportation on geometric domains. *ACM Trans. Graph.*, 2015. 2, 3
- [64] Jiaming Song, Chenlin Meng, and Stefano Ermon. Denoising diffusion implicit models. *arXiv preprint arXiv:2010.02502*, 2020. 1, 3
- [65] Yang Song, Jascha Sohl-Dickstein, Diederik P Kingma, Abhishek Kumar, Stefano Ermon, and Ben Poole. Score-based generative modeling through stochastic differential equations. *arXiv preprint arXiv:2011.13456*, 2020. 1, 3
- [66] Mingze Sun, Chen Guo, Puhua Jiang, Shiwei Mao, Yurun Chen, and Ruqi Huang. Srif: Semantic shape registration empowered by diffusion-based image morphing and flow estimation. In *ACM SIGGRAPH*, 2024. 3
- [67] Gary KL Tam, Zhi-Quan Cheng, Yu-Kun Lai, Frank C Langbein, Yonghuai Liu, David Marshall, Ralph R Martin, Xian-Fang Sun, and Paul L Rosin. Registration of 3d point clouds and meshes: A survey from rigid to nonrigid. *IEEE Trans. Vis. Comput. Graph.*, 2012. 2, 3
- [68] Jiaxiang Tang, Zhaoxi Chen, Xiaokang Chen, Tengfei Wang, Gang Zeng, and Ziwei Liu. Lgm: Large multi-view gaussian model for high-resolution 3d content creation. In *Proc. Eur. Conf. Comput. Vis.*, 2024. 2, 3
- [69] Dmitry Tochilkin, David Pankratz, Zexiang Liu, Zixuan Huang, Adam Letts, Yangguang Li, Ding Liang, Christian Laforte, Varun Jampani, and Yan-Pei Cao. Triposr: Fast 3d object reconstruction from a single image. *arXiv preprint arXiv:2403.02151*, 2024. 3
- [70] Chih-Jung Tsai, Cheng Sun, and Hwann-Tzong Chen. Multiview regenerative morphing with dual flows. In *Proc. Eur. Conf. Comput. Vis.*, 2022. 1, 3, 6, 7, 13
- [71] Laurens Van der Maaten and Geoffrey Hinton. Visualizing data using t-sne. *Journal of machine learning research*, 2008. 5
- [72] Oliver Van Kaick, Hao Zhang, Ghassan Hamarneh, and Daniel Cohen-Or. A survey on shape correspondence. In *Comput. Graph. Forum*, 2011. 2, 3
- [73] Ashish Vaswani, Noam Shazeer, Niki Parmar, Jakob Uszkoreit, Llion Jones, Aidan N Gomez, Łukasz Kaiser, and Illia Polosukhin. Attention is all you need. In *Adv. Neural Inf. Process. Syst.*, 2017. 3
- [74] Clinton J Wang and Polina Golland. Interpolating between images with diffusion models. *arXiv preprint arXiv:2307.12560*, 2023. 3
- [75] Zhengyi Wang, Yikai Wang, Yifei Chen, Chendong Xiang, Shuo Chen, Dajiang Yu, Chongxuan Li, Hang Su, and Jun Zhu. Crm: Single image to 3d textured mesh with convolutional reconstruction model. In *Proc. Eur. Conf. Comput. Vis.*, 2024. 3
- [76] Zehan Wang, Ziang Zhang, Tianyu Pang, Chao Du, Hengshuang Zhao, and Zhou Zhao. Orient anything: Learning robust object orientation estimation from rendering 3d models. *arXiv preprint arXiv:2412.18605*, 2024. 6
- [77] George Wolberg. Recent advances in image morphing. *Proceedings of CG International'96*, 1996. 1
- [78] George Wolberg. Image morphing: a survey. *The visual computer*, 1998. 1
- [79] Kailu Wu, Fangfu Liu, Zhihan Cai, Runjie Yan, Hanyang Wang, Yating Hu, Yueqi Duan, and Kaisheng Ma. Unique3d: High-quality and efficient 3d mesh generation from a single image. In *Adv. Neural Inf. Process. Syst.*, 2024. 3
- [80] Shuang Wu, Youtian Lin, Feihu Zhang, Yifei Zeng, Jingxi Xu, Philip Torr, Xun Cao, and Yao Yao. Direct3d: Scalable image-to-3d generation via 3d latent diffusion transformer. In *Adv. Neural Inf. Process. Syst.*, 2024. 2
- [81] Shuang Wu, Youtian Lin, Feihu Zhang, Yifei Zeng, Yikang Yang, Yajie Bao, Jiachen Qian, Siyu Zhu, Xun Cao, Philip Torr, et al. Direct3d-s2: Gigascale 3d generation made easy with spatial sparse attention. *arXiv preprint arXiv:2505.17412*, 2025.
- [82] Jianfeng Xiang, Zelong Lv, Sicheng Xu, Yu Deng, Ruicheng Wang, Bowen Zhang, Dong Chen, Xin Tong, and Jiaolong Yang. Structured 3d latents for scalable and versatile 3d generation. In *Proc. IEEE Conf. Comput. Vis. Pattern Recogn.*, 2025. 2, 3, 6, 8, 13, 14
- [83] Jiale Xu, Weihao Cheng, Yiming Gao, Xintao Wang, Shenghua Gao, and Ying Shan. Instantmesh: Efficient 3d mesh generation from a single image with sparse-view large reconstruction models. *arXiv preprint arXiv:2404.07191*, 2024. 3
- [84] Songlin Yang, Yushi Lan, Honghua Chen, and Xingang Pan. Textured 3d regenerative morphing with 3d diffusion prior. *arXiv preprint arXiv:2502.14316*, 2025. 1, 2, 3, 4, 6, 14
- [85] Xianghui Yang, Huiwen Shi, Bowen Zhang, Fan Yang, Jiacheng Wang, Hongxu Zhao, Xinhai Liu, Xinzhou Wang, Qingxiang Lin, Jiaao Yu, et al. Hunyuan3d 1.0: A unified framework for text-to-3d and image-to-3d generation. *arXiv preprint arXiv:2411.02293*, 2024. 3
- [86] Zhaoyuan Yang, Zhengyang Yu, Zhiwei Xu, Jaskirat Singh, Jing Zhang, Dylan Campbell, Peter Tu, and Richard

- Hartley. Impus: Image morphing with perceptually-uniform sampling using diffusion models. *arXiv preprint arXiv:2311.06792*, 2023. [3](#)
- [87] Chongjie Ye, Yushuang Wu, Ziteng Lu, Jiahao Chang, Xiaoyang Guo, Jiaqing Zhou, Hao Zhao, and Xiaoguang Han. Hi3dgen: High-fidelity 3d geometry generation from images via normal bridging. In *Proc. IEEE Int. Conf. Comput. Vis.*, 2025. [3](#), [8](#), [14](#)
- [88] Junliang Ye, Shenghao Xie, Ruowen Zhao, Zhengyi Wang, Hongyu Yan, Wenqiang Zu, Lei Ma, and Jun Zhu. Nano3d: A training-free approach for efficient 3d editing without masks. *arXiv preprint arXiv:2510.15019*, 2025. [2](#), [3](#)
- [89] Biao Zhang, Jiapeng Tang, Matthias Nießner, and Peter Wonka. 3dshape2vecset: A 3d shape representation for neural fields and generative diffusion models. *ACM Trans. Graph.*, 2023. [2](#), [3](#)
- [90] Bowen Zhang, Yiji Cheng, Jiaolong Yang, Chunyu Wang, Feng Zhao, Yansong Tang, Dong Chen, and Baining Guo. Gaussiancube: A structured and explicit radiance representation for 3d generative modeling. *arXiv preprint arXiv:2403.19655*, 2024. [3](#)
- [91] Kaiwen Zhang, Yifan Zhou, Xudong Xu, Bo Dai, and Xingang Pan. Diffmorpher: Unleashing the capability of diffusion models for image morphing. In *Proc. IEEE Conf. Comput. Vis. Pattern Recogn.*, 2024. [1](#), [2](#), [3](#), [4](#), [6](#), [7](#), [13](#)
- [92] Longwen Zhang, Ziyu Wang, Qixuan Zhang, Qiwei Qiu, Anqi Pang, Haoran Jiang, Wei Yang, Lan Xu, and Jingyi Yu. Clay: A controllable large-scale generative model for creating high-quality 3d assets. *ACM Trans. Graph.*, 2024. [2](#), [3](#)
- [93] Zibo Zhao, Wen Liu, Xin Chen, Xianfang Zeng, Rui Wang, Pei Cheng, Bin Fu, Tao Chen, Gang Yu, and Shenghua Gao. Michelangelo: Conditional 3d shape generation based on shape-image-text aligned latent representation. In *Adv. Neural Inf. Process. Syst.*, 2023.
- [94] Zibo Zhao, Zeqiang Lai, Qingxiang Lin, Yunfei Zhao, Haolin Liu, Shuhui Yang, Yifei Feng, Mingxin Yang, Sheng Zhang, Xianghui Yang, et al. Hunyuan3d 2.0: Scaling diffusion models for high resolution textured 3d assets generation. *arXiv preprint arXiv:2501.12202*, 2025. [2](#), [3](#)
- [95] Junzhe Zhu, Yuanchen Ju, Junyi Zhang, Muhan Wang, Zhecheng Yuan, Kaizhe Hu, and Huazhe Xu. Densematcher: Learning 3d semantic correspondence for category-level manipulation from a single demo. *arXiv preprint arXiv:2412.05268*, 2024. [3](#), [6](#), [7](#), [13](#)
- [96] Lei Zhu, Yan Yang, Steven Haker, and Allen Tannenbaum. An image morphing technique based on optimal mass preserving mapping. *IEEE Trans. Image Process.*, 2007. [2](#)

## 6. Supplemental Material Overview

This document includes the following supplementary sections:

- Initialization Details.
- Additional Experimental Details.
- Extended 3D Morphing Results.
- Additional Qualitative Experiments.
- Additional Application Details.
- Generalization Details.

## 7. Initialization Details

**3D Inversion.** For real-world assets, initial noisy latents  $f_{\text{init}}$  and image conditions  $c$  are obtained via 3D inversion, following the procedure in VoxHammer [37]. This involves two stages: Sparse Structure (SS) and Structured Latent (SLAT), which map a 3D asset to its corresponding initial latents  $f_{\text{init\_ss}}$  and  $f_{\text{init\_slat}}$ . Further implementation details are provided in Sec. 3.2 of VoxHammer [37].

**Initial Features Interpolation.** The initial feature for frame  $n$ ,  $f_{\text{init}}^n$ , is computed by spherical interpolation [91] with a deformation weight  $\alpha^n \in [0, 1]$ , ensuring  $x^0 = x^{\text{src}} (\alpha^0 = 0)$  and  $x^N = x^{\text{tgt}} (\alpha^N = 1)$ . Specifically, we obtain the initial features in the SS stage of source and target assets via 3D inversion, denoted as  $f_{\text{init\_ss}}^{\text{src}}$  and  $f_{\text{init\_ss}}^{\text{tgt}}$ . The initial feature in the SS stage for frame  $n$  is calculated as:

$$f_{\text{init\_ss}}^n = \frac{\sin((1 - \alpha^n)\theta)}{\sin(\theta)} f_{\text{init\_ss}}^{\text{src}} + \frac{\sin(\alpha^n\theta)}{\sin(\theta)} f_{\text{init\_ss}}^{\text{tgt}}, \quad (5)$$

where  $\theta = \arccos\left(\frac{f_{\text{init\_ss}}^{\text{src}} \cdot f_{\text{init\_ss}}^{\text{tgt}}}{\|f_{\text{init\_ss}}^{\text{src}}\| \|f_{\text{init\_ss}}^{\text{tgt}}\|}\right)$ . A similar approach is used for the SLAT stage, but requires finding corresponding sparse voxels based on Euclidean distance before performing spherical interpolation.

## 8. Additional Experimental Details

**Implementation Details.** Our method builds upon Image-to-3D Trellis [82], replacing all cross-attention modules with our proposed Morphing Cross-Attention (MCA) modules and self-attention modules with Temporal-Fused Self-Attention (TFSA) modules. After obtaining the structure of the  $n$ -th frame  $P^n$ , orientation correction is performed. All modules introduced require no training, allowing flexible and cost-effective application to other SLAT-based models. Both stages use a sampling step of 25 and a classifier-free guidance (CFG) guidance scale of 5.0.

**Baselines Implementation Details.** (1) 3DInterp and SLTAInterp: We first establish correspondence between the target and source objects using a well-known 3D shape correspondence method, DenseMatcher [95] (ICLR 2025, Spotlight). We then perform interpolation directly on the corresponding 3D-representation or SLAT-representation to



You are a professional reviewer specializing in digital art and 3D design. Multiple sets of 3D assets—depicting the same subject—have been generated using different methods (e.g., NeRF, 3D Gaussian Splatting, diffusion-based 3D generation, etc.). Evaluate these results based on the following aesthetic criteria:

- (1) Overall harmony: balance, proportion, and structural coherence
- (2) Surface detail and texture: richness, realism, and material fidelity
- (3) Consistency of artistic style: unity and intentionality in visual language
- (4) Visual appeal: immediate aesthetic impact and emotional resonance

Identify the method that produces the most aesthetically pleasing asset, and justify your selection with specific observations tied to the criteria above. Focus exclusively on perceptual and artistic quality, not technical efficiency or computational cost.



The asset on the far left likely represents the output of the highest-quality. The subsequent assets (moving right) demonstrate a clear and rapid degradation of quality, which are likely artifacts or incomplete results from less stable methods:

- (1) The second asset is a blurry, amorphous blob, lacking any discernible detail or structure—a common failure state or low-iteration output.
- (2) The third and fourth assets (the vehicles with the large wheels/engines) retain structural information but suffer from color noise, smearing, and a complete breakdown of material definition, suggesting a loss of texture fidelity.
- (3) The final three assets are increasingly fragmented, showing a breakdown of the 3D representation into scattered points or colored clumps, demonstrating a total failure of overall harmony and consistency of artistic style.

Therefore, the first asset on the far left is the clear winner because it is the only one that fully satisfies all four aesthetic criteria with a high degree of quality and completeness.



Figure 13. Examples of Aesthetics Score (AS) evaluation using vision-language models Gemini-2.5 [26] and ChatGPT-5 [51]. Given rendered images of morphed 3D assets, the models select the most aesthetically pleasing result across all methods.

generate the morphed 3D results. (2) DiffMorpher [91] and FreeMorph [4]: We use their officially released code to obtain 2D morphing results. Subsequently, we generate the final 3D assets from the morphed images using Image-to-3D Trellis [82]. (3) MorphFlow [70]: We first render multi-view images of the source and target 3D assets. Their official code is then used to generate the final morphed results.

**Evaluation Metrics Details.** (1) Fréchet Inception Distance (FID) [29]: For each morphed asset and its originals, we render 12 images uniformly sampled along the yaw axis and compute FID between the rendered distributions. (2) Perceptual Path Length (PPL) and Perceptual Distance Variance (PDV) [91]: For each source-target pair, we render six morphing videos (uniform yaw views) and compute PPL/PDV as in DiffMorpher [91]. (3) Aesthetics Scores (AS): Using Gemini-2.5 [26] and ChatGPT-5 [51], we prompt the models to select the most visually appealing morphed asset per pair (see Fig. 13). AS is the selection frequency (as a percentage). (4) User Preference (UP): We conducted a user study with 49 participants experienced in computer vision and graphics. They selected their preferred result across 10 source-target pairs based on quality, smoothness, and realism (see Fig. 18). UP is reported as the selection percentage.

## 9. Extended 3D Morphing Results

Additional results are shown in Figs. 19 and 20. Our method produces high-quality, smooth morphs across diverse categories—including animals, vehicles, buildings, and hu-

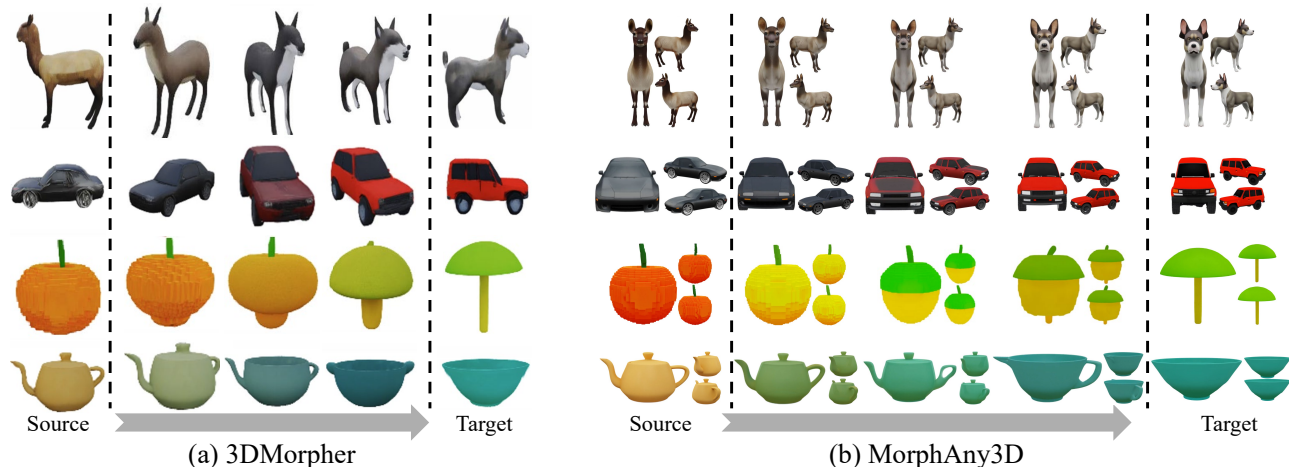


Figure 14. Qualitative comparison with 3DMorpher [84]. Results from 3DMorpher are reproduced directly from their published paper.



Figure 15. Disentangled 3D morphing. By applying our Morphing Cross-Attention (MCA) and Temporal-Fused Self-Attention (TFSA) modules exclusively in one stage (SS or SLAT), we independently control structural and detail deformation.

manoids. We visualize RGB renders from the 3DGS representation and normal maps from the mesh to highlight both appearance and geometric fidelity.

## 10. Additional Qualitative Experiments

Further comparisons appear in Figs. 21 and 22. Our method consistently outperforms baselines in morphing quality and temporal smoothness. Since 3DMorpher [84] has not released full code, we compare qualitatively using results reproduced from their paper (Fig. 14). We use the same source and target assets: cropped images from their figures are lifted to 3D via Image-to-3D Trellis [82]. As shown, our results exhibit superior detail and coherence. Moreover, 3DMorpher struggles with complex structures (e.g., Figs. 19 and 20) and relies solely on 3DGS, which lacks high-fidelity normals and compatibility with standard 3D software [1, 24].

## 11. Additional Application Details

**Disentangled 3D Morphing.** Thanks to Trellis’s decoupled SS and SLAT stages, our method supports disentangled morphing. As illustrated in Fig. 15:

- Structure-only morphing: Apply MCA/TFSA only in the SS stage to deform global shape while preserving local

details.

- Detail-only morphing: Apply MCA/TFSA only in the SLAT stage to transfer texture and fine geometry without altering overall structure.

**Dual-Target 3D Morphing.** As shown in Fig. 16, distinct targets can be assigned to each stage: the SS stage adopts the source’s global shape from one target, while the SLAT stage incorporates local details from another target. This enables flexible composition of 3D assets, blending shapes and details from different sources.

**3D Style Transfer.** By conditioning the SLAT stage on a style reference while keeping the SS stage fixed to the source structure, our method performs 3D style transfer (Fig. 17), preserving shape while adopting the reference’s geometric and textural style.

## 12. Generalization Details

Hi3DGen [87]—a recent SLAT-based method for high-fidelity 3D generation—uses the same Trellis framework and image conditioning. Thus, our approach applies directly without retraining. Since Hi3DGen focuses on geometry (no texture), we report only normal maps.

For Text-to-3D Trellis [82], we replace image conditions in MCA with textual prompts. No other changes are needed, enabling zero-shot adaptation. However, textual conditions

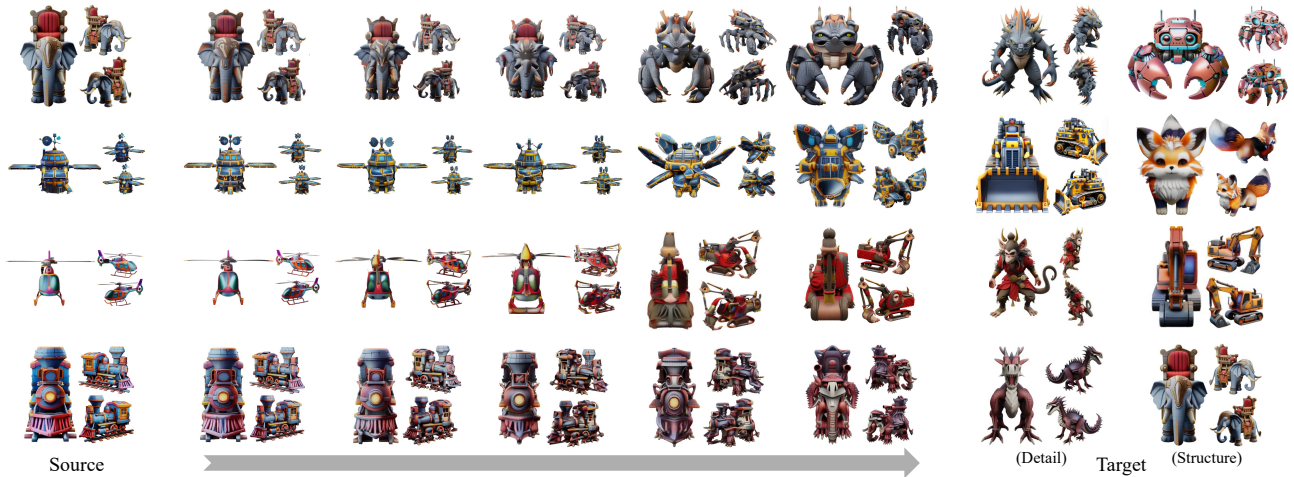


Figure 16. Dual-target 3D morphing. Distinct target assets are assigned to the SS and SLAT stages, enabling flexible composition of global shape and local details from two different sources.



Figure 17. 3D style transfer. A style reference guides the SLAT stage while the SS stage retains the source structure, allowing texture and geometric style to be transferred without altering the underlying shape.

are more abstract than visual ones, leading to reduced deformation quality and temporal coherence. We therefore recommend image-guided SLAT models when possible.

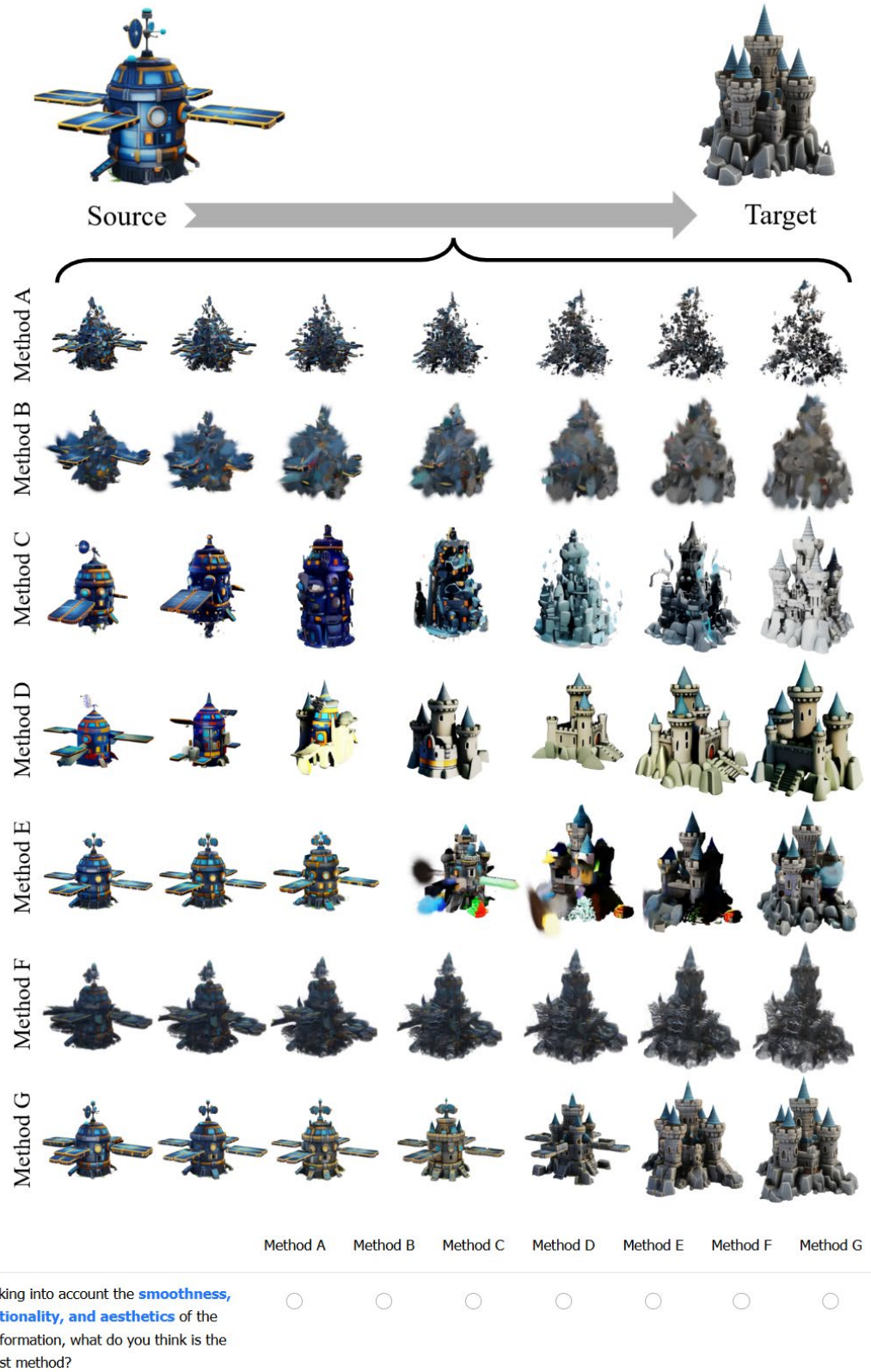


Figure 18. User Preference (UP) evaluation. Participants selected their preferred morphed 3D asset from all methods based on rendered images, judging quality, smoothness, and realism.



Figure 19. Extended 3D morphing results across diverse object categories (e.g., animals, vehicles, buildings). Our method produces high-fidelity and temporally smooth transitions.

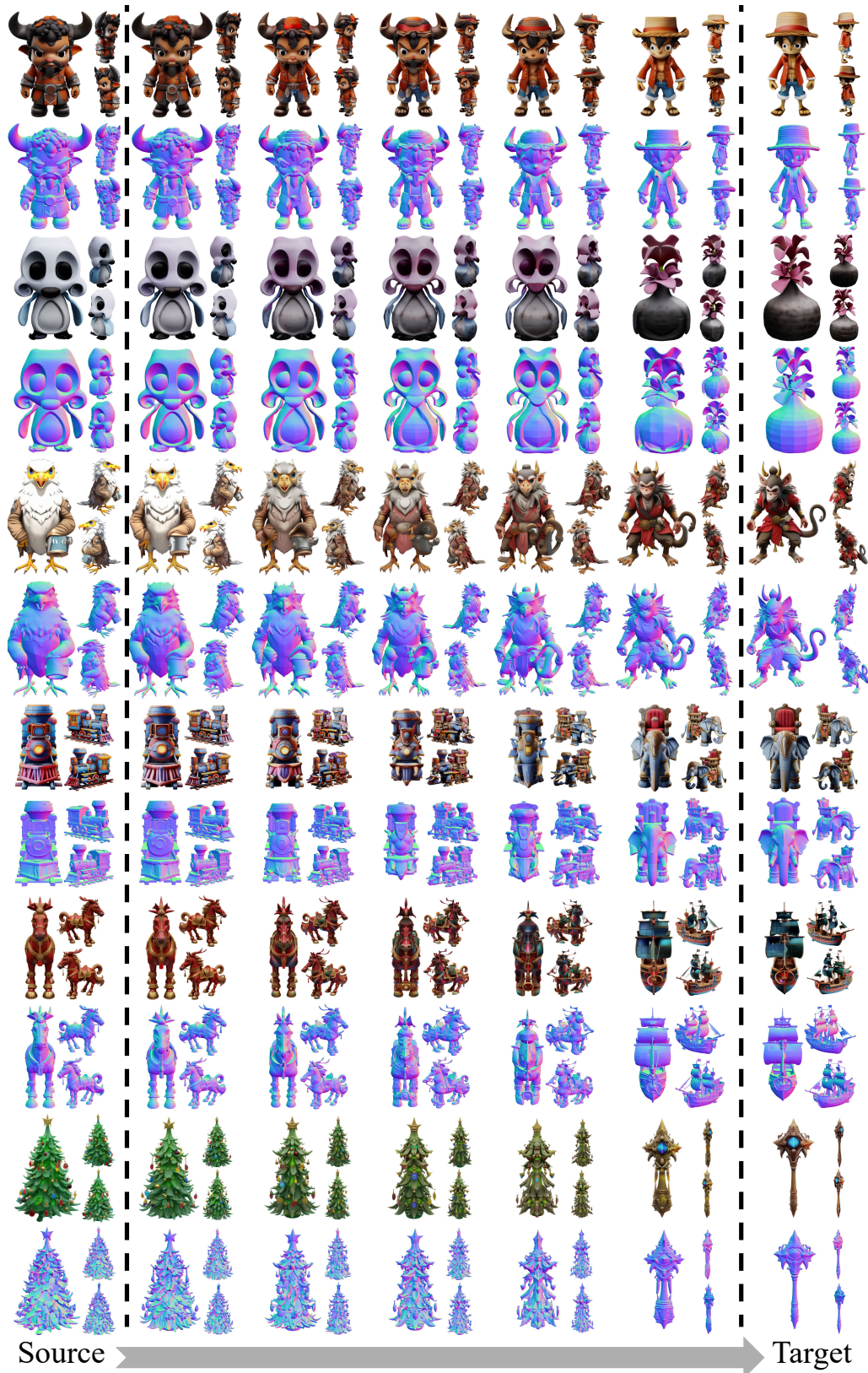


Figure 20. Additional extended results demonstrating consistent morphing quality across varied and challenging object categories.

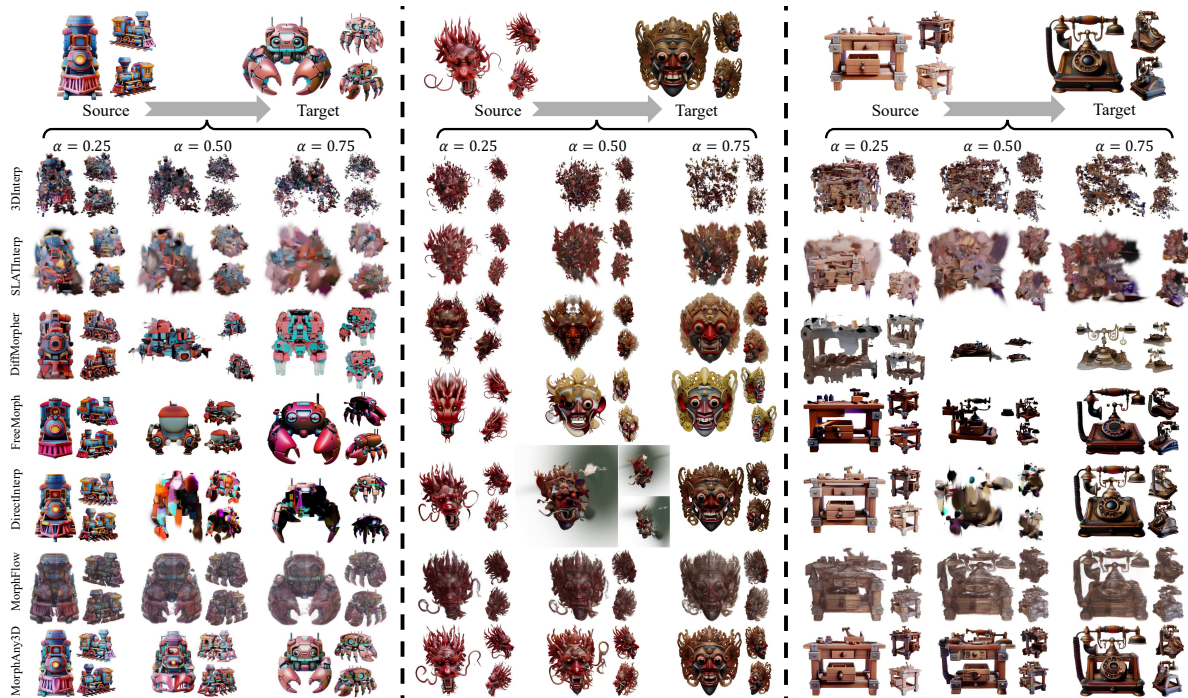


Figure 21. Qualitative comparison with baseline methods. Our approach achieves superior morphing quality and smoother transitions.

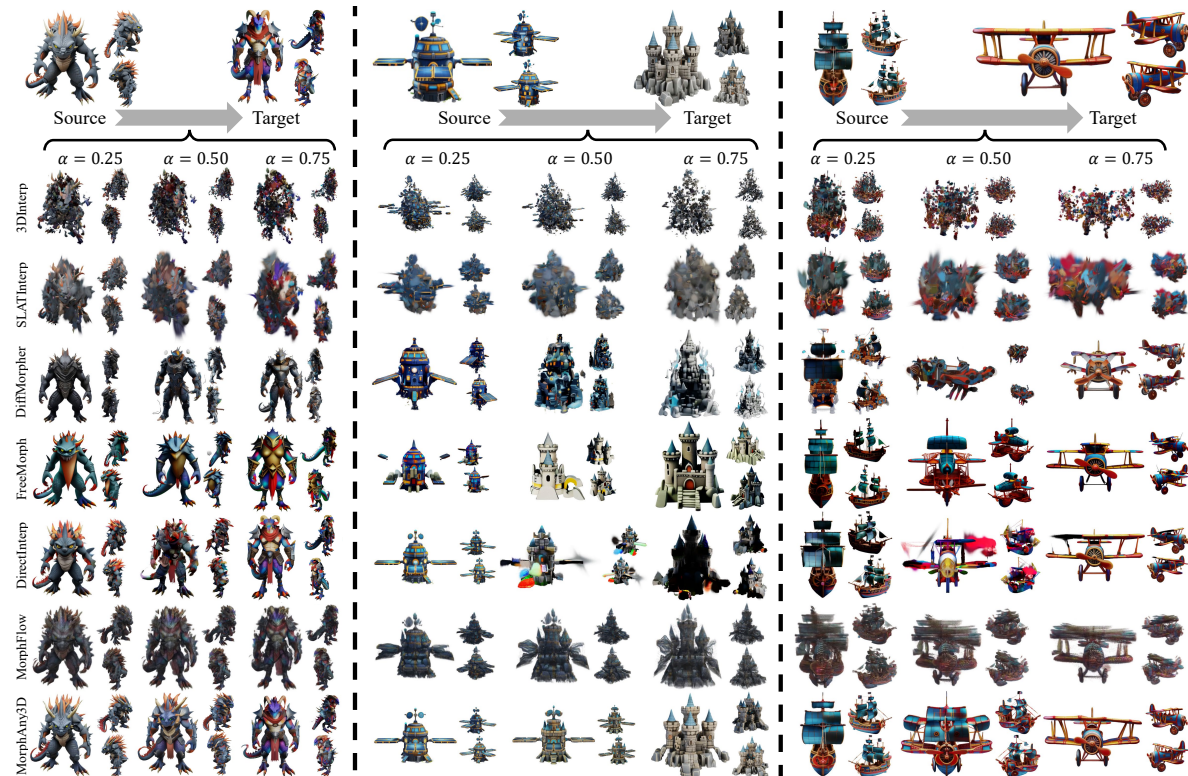


Figure 22. Further qualitative comparisons highlighting the advantages of our method over existing approaches in preserving geometry and ensuring temporal coherence.